# Apparent horizon finder for general three-dimensional spaces

Masaru Shibata
*Department of Physics, University of Illinois at Urbana-Champaign, Urbana, Illinois 61801*
*and Department of Earth and Space Science, Graduate School of Science, Osaka University, Toyonaka, Osaka 560-0043, Japan*

Kōji Uryū
*SISSA, Via Beirut 2/4, 34013 Trieste, Italy*

(Received 18 November 1999; published 25 September 2000)

We present a numerical method for finding the apparent horizon in general three-dimensional (3D) spaces without any symmetries for 3D numerical relativity. We apply this method for black hole spacetimes to demonstrate its quick convergence to solutions and reasonable accuracy.

PACS number(s): 04.25.Dm

## I. INTRODUCTION

In Ref. [1], Shibata presented a method for determining the two-surface of the apparent horizons for a special family of 3D spaces in which the system has certain symmetries (e.g., $\pi$-rotation symmetry around the $z$ axis and plane symmetry with respect to the equatorial plane). In this method, a matrix equation is derived by taking the finite differencing of an elliptic-type equation for the two-surface of the apparent horizon [see Eq. (2.1)]. Then, the matrix equation is solved iteratively until a sufficient convergence is achieved. This is in contrast with other popular methods proposed so far in which spectrum decompositions are introduced [2–5] (see also other approaches in [6,7]). This apparent horizon finder has been used in recent 3D numerical simulations to determine black hole formation at the late stage of merger between two identical neutron stars or clusters of equal mass and spin [8] as well as gravitational collapses of rotating neutron stars or ellipsoids [9]. It, however, cannot be applied to problems in which no symmetries exist such as the merger between two neutron stars of unequal mass or the merger of a black-hole–neutron-star binary to form a black hole.

Recently, we have become aware of a way to extend our previous code for general 3D spaces of no symmetries. In this Brief Report, we describe a method for improvement as an addendum of [1], and present the numerical results for the test problems to show the robustness. In Sec. II, we describe the numerical method for finding the apparent horizon. In Sec. III, numerical results for some test problems are presented. Section IV is devoted to a summary.

## II. METHOD

We assume that the two-surface of an apparent horizon is expressed by $h(\varphi,\theta)$ where $\varphi$ and $\theta$ denote angles in appropriately defined spherical polar coordinates [10]. Then, we write the equation for the apparent horizon in the form [1]

$$\frac{\partial^2 h}{\partial\theta^2}+\cot\theta\frac{\partial h}{\partial\theta}+\frac{1}{\sin^2\theta}\frac{\partial^2 h}{\partial\varphi^2}-2h=S, \tag{2.1}$$

where $S$ is composed of geometric variables and complicated function of $h$ (see, e.g., Ref. [1]). Following [1], we take the grid points in numerical computation as

$$\varphi_i=\left(i-\frac{1}{2}\right)\Delta\varphi,\quad i=1,2,\ldots,N_\varphi, \tag{2.2}$$

$$\theta_j=\left(j-\frac{1}{2}\right)\Delta\theta,\quad j=1,2,\ldots,N_\theta, \tag{2.3}$$

where $N_\varphi$ and $N_\theta$ denote the grid numbers in $\varphi$ and $\theta$ directions, respectively, and by them, we can define $\Delta\varphi\equiv 2\pi/N_\varphi$ and $\Delta\theta\equiv\pi/N_\theta$. Then, we search for the solution for $h(i,j)$ of $1\leqslant i\leqslant N_\varphi$ and $1\leqslant j\leqslant N_\theta$.

The matrix equation for $h_k$ $[k=i+(j-1)N_\varphi]$ is derived by taking the standard second-order finite differencing for Eq. (2.1) as

$$\frac{\partial^2 h}{\partial\theta^2}=\frac{h(i,j+1)-2h(i,j)+h(i,j-1)}{\Delta\theta^2}, \tag{2.4}$$

$$\frac{\partial h}{\partial\theta}=\frac{h(i,j+1)-h(i,j-1)}{2\Delta\theta}, \tag{2.5}$$

$$\frac{\partial^2 h}{\partial\varphi^2}=\frac{h(i+1,j)-2h(i,j)+h(i-1,j)}{\Delta\varphi^2}. \tag{2.6}$$

Here, at $i=1$ and $N_\varphi$ and $j=1$ and $N_\theta$, there appear the terms at dummy points, $h(0,j)$, $h(N_\varphi+1,j)$, $h(i,0)$, and $h(i,N_\theta+1)$, which are not defined in Eqs. (2.2) and (2.3). To obtain the matrix equation, we need appropriate conditions to replace them with $h(i,j)$ of $1\leqslant i\leqslant N_\varphi$ and $1\leqslant j\leqslant N_\theta$. For the former two, we may use the conditions $h(0,j)=h(N_\varphi,j)$ and $h(N_\varphi+1,j)=h(1,j)$ because the $2\pi$-rotation symmetry holds in any 3D space. On the other hand, we have not been aware of boundary conditions for the latter two in general 3D spaces of no symmetries. This was one of the reasons that we previously restricted our study to a special family of 3D spaces [1] in which we could adopt the boundary condition $\partial h/\partial\theta=0$ at $\theta=0$ and $\pi$ (or $\pi/2$) and use the relations $h(i,0)=h(i,1)$ and $h(i,N_\theta+1)=h(i,N_\theta)$ to obtain the matrix equation.

 

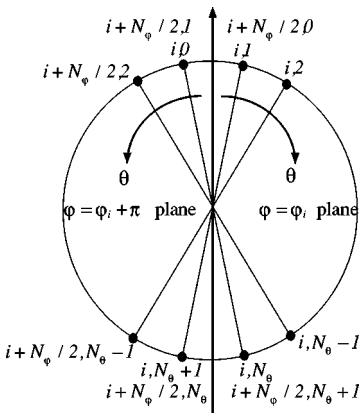


FIG. 1. Schematic figure for the location of grid points for $\theta_j$ in $\varphi_i$ and $\varphi_i+\pi$ planes with $\varphi_i$ being constant. The figure shows that the dummy points $(i,0)$ and $(i,N_\theta+1)$ coincide with the regular points $(i+N_\varphi/2,1)$ and $(i+N_\varphi/2,N_\theta)$, respectively. Note that in this figure we assume $1\leqslant i\leqslant N_\varphi/2$.

However, there is no such difficulty in reality. $h(i,0)$ and $h(i,N_\theta+1)$ can be replaced with other $h(i,j)$ in the regular grid points because we may recognize that the dummy points $(i,0)$ and $(i,N_\theta+1)$ are located at the same points as $(i\pm N_\varphi/2,1)$ and $(i\pm N_\varphi/2,N_\theta)$, respectively (see Fig. 1); i.e., we can use the relations

$$h(i,0)=\begin{cases} h(i+N_\varphi/2,1) & 1\leqslant i\leqslant N_\varphi/2, \\ h(i-N_\varphi/2,1) & N_\varphi/2+1\leqslant i\leqslant N_\varphi, \end{cases} \tag{2.7}$$

$$h(i,N_\theta+1)=\begin{cases} h(i+N_\varphi/2,N_\theta) & 1\leqslant i\leqslant N_\varphi/2, \\ h(i-N_\varphi/2,N_\theta) & N_\varphi/2+1\leqslant i\leqslant N_\varphi. \end{cases} \tag{2.8}$$

Therefore, the matrix equation for $h_k$ is constructed in a straightforward manner even in the general 3D spaces of no symmetries.

In the numerical implementation, we move the terms $h(i,0)-h(i,1)$ and $h(i,N_\theta+1)-h(i,N_\theta)$, which appear on the left-hand side of Eq. (2.1) at $j=1$ and $N_\theta$ and do not vanish unless $\partial h/\partial\theta=0$, to the right-hand side and apply Eqs. (2.7) and (2.8). Then, Eq. (2.1) is reduced to the matrix equation in the form $M_{lk}h_k=\tilde{S}_l$ $[k,l=i+(j-1)N_\varphi]$ where $1\leqslant l,k\leqslant N_\varphi\times N_\theta$ and the matrix $M_{lk}$ has the same form as that adopted in [1] [see Eq. (2.20) of [1]]. We can use the same numerical method as that adopted in [1] for solving the matrix equation iteratively. One concern is whether the regularity is maintained around $\theta=0$ and $\pi$ in this method because there appear many terms of $\sin^{-n}\theta$ $(n=1,2)$ in Eq. (2.1). In the next section, we demonstrate that it does not matter and our new scheme can capture a highly distorted apparent horizon.

## III. NUMERICAL TESTS

Throughout this paper, we assume that the three-space has the conformal flat line element as

$$dl^2=\psi^4\eta_{ij}dx^idx^j, \tag{3.1}$$

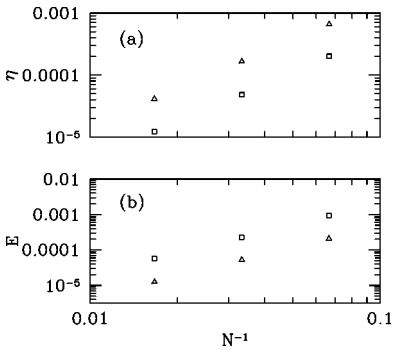


FIG. 2. $\eta$ and $E$ as a function of $N^{-1}$ for $a/M=0.1$ (triangles) and 0.2 (squares) for a shifted Schwarzschild black hole.

where $\eta_{ij}$ denotes the flat spatial metric, and $\psi$ satisfies an elliptic-type equation which is derived from the Hamiltonian constraint (e.g., [1]). In the following numerical experiments, we set $N_\varphi=2N_\theta\equiv 2N$ and change $N$ to investigate the convergence.

As a first step, we pay attention to the time-symmetric, vacuum 3D spaces; i.e., extrinsic curvature $K_{ij}$ is vanishing. Following Nakamura, Kojima, and Oohara [2], we first apply our apparent horizon finder to the shifted Schwarzschild black hole in which

$$\psi=1+\frac{M}{2|\mathbf{x}-\mathbf{x}_0|}, \tag{3.2}$$

where $M$ is the gravitational mass of the system [11] and $\mathbf{x}_0$ is the nonzero vector. In this case, the apparent horizon is located at $|\mathbf{x}-\mathbf{x}_0|=M/2$ with the area $A=16\pi M^2$. Here, we choose $\mathbf{x}_0=(a,a,a/2)$ as an example. In this test, we choose $\varphi$ and $\theta$ which are identical with those of the background coordinates $\mathbf{x}$ (hereafter we denote them as $\bar{\varphi}$ and $\bar{\theta}$). As an initial guess, we simply give $h(i,j)=M$. Hereafter, we judge that the convergence to a numerical solution is achieved when the difference of a norm $\Sigma_{i,j}h(i,j)^2$ for next two iteration steps becomes less than $10^{-8}$.

In Fig. 2(a), we show

$$\eta\equiv 1-\sqrt{\frac{A}{16\pi M^2}} \tag{3.3}$$

as a function of $N^{-1}$ for $a/M=0.1$ and 0.2. In this 3D space, $\eta$ is zero for exact $h$ so that $\eta$ may be regarded as the measure of the error for $A$. In Fig. 2(b), we also show an error of the solution defined as

$$E\equiv\frac{1}{N_\theta N_\varphi M}\sum_{i=1}^{N_\varphi}\sum_{j=1}^{N_\theta}|h(i,j)-h_e(i,j)|, \tag{3.4}$$

where $h_e(i,j)$ is the exact solution. In this experiment, we choose $N=15$, 30, and 60. As is shown in Fig. 2, $\eta$ and $E$ decrease in proportion to $N^{-2}$, which shows that the second-order convergence is achieved in our code.

Within $\sim 30$ iteration steps, the convergence to a numerical solution is achieved for $a\lesssim 0.1M$. The number of iteration steps increases with increasing $a$, but it is at most $\sim 50$

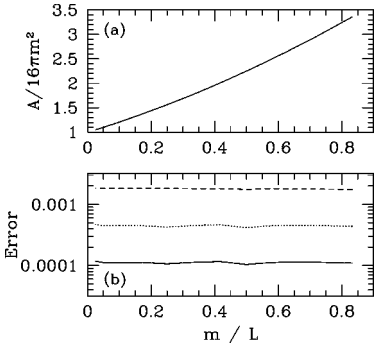


FIG. 3. (a) Area of the apparent horizon in units of $16\pi m^2$ for one of three black holes as a function of $m/L$. (b) The error for estimation of the area as a function of $m/L$ for $N=15$ (dashed line), 30 (dotted line), and 60 (solid line).

even for $a=0.2M$. These facts imply that even if the initial guess is not very good, the convergence is achieved fairly quickly. The computational time per one iteration is typically 0.1 CPU second using a FACOM VX/4R machine even for the $N=60$ case, which will occupy a tiny fraction in our 3D simulation in full general relativity [8].

We note that even for the case $a=0.2M$, the apparent horizon is determined accurately. This implies that the origin of the coordinate system for $(\varphi,\theta)$ may highly deviate from the centers of the black hole. This will be a desirable property because the location of the center of a black hole is in general not clear in 3D numerical simulations.

Next, we apply the apparent horizon finder to a 3D space of three black holes of equal mass $m$ (i.e., the total gravitational mass $M$ is $3m$). For simplicity, we choose $\psi$ in the Brill-Lindquist form [12]

$$\psi=1+\frac{m}{2}\sum_{n=1}^{3}\frac{1}{|\mathbf{x}-\mathbf{x}_n|}. \tag{3.5}$$

Here, we locate $\mathbf{x}_n$ at the vertex of an equilateral triangle. We choose $\mathbf{x}_n$ as $(L/2,\pm L/2,0)$ and $(L(1-\sqrt{3})/2,0,0)$ where $L$ denotes the coordinate length of the side of the triangle. Although the system has the plane symmetries with respect to the $y=0$ and $z=0$ planes, we solve Eq. (2.1) without imposing these symmetries in numerical experiment.

As shown by Oohara *et al.* [3], only the apparent horizons for encompassing individual black hole exist for the case when $L$ is large enough. On the other hand, if $L$ is small enough, the common apparent horizon encompassing all the black holes exists. Hereafter, we search for the common apparent horizon with $(\varphi,\theta)=(\overline{\varphi},\overline{\theta})$ and from an initial guess for the solution as $h_k=2m$. For the smaller apparent horizon encompassing one black hole, we define $(\varphi,\theta)$ so that the origin is at $\mathbf{x}=\mathbf{x}_n$ and give the initial guess as $h_k=0.5m$. Irrespective of $L$, the apparent horizon for the smaller hole is determined with $\sim 30$ iteration steps. On the other hand, the iteration steps increase with increasing $L$ for determining the common apparent horizon. For $L\sim 1.5m$, $\sim 40$ iteration steps are enough, but for $L\gtrsim 2m$, more than 100 iteration steps are necessary.

In Fig. 3(a), we show the area of the apparent horizon

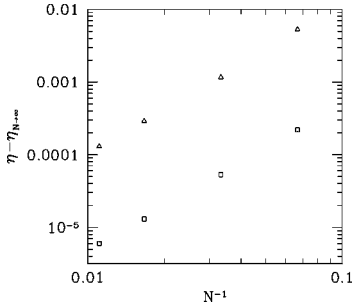


FIG. 4. Error for estimation of $\eta$ as a function of $N^{-1}$ for $L=1.5m$ (squares) and $2m$ (triangles) for three black holes.

$A_{\rm one}$ in units of $16\pi m^2$ for one of three black holes as a function of $m/L$. We perform the computation changing $N$ as 15 (dotted line), 30 (dashed line), and 60 (solid line), and derive the extrapolated value in the limit $N\to\infty$ assuming that the numerical results for $N$ behave as $A_{\rm one}(N)=A_{\rm one}+CN^{-2}$ where $C$ is a constant. We find that $A_{\rm one}$ is in good agreement of the previous result presented in [3]. In Fig. 3(b), we show the error for estimation of the area defined as

$$\left|1-\frac{A_{\rm one}(N)}{A_{\rm one}}\right|, \tag{3.6}$$

for $N=15$ (dashed line), 30 (dotted line), and 60 (solid line). We find that the numerical results are second-order convergent irrespective of $L$ and that the area is obtained within 0.2% error even for $N=15$.

Next, we determine the maximum allowed value of $L$, $L_{\rm crit}$, for the existence of the common apparent horizon changing $N$. We find that $L_{\rm crit}/m=2.02$ for $N=15$, 2.04 for $N=30$ and 60, and 2.05 for $N=90$. Thus, it is expected that $L_{\rm crit}$ is $\simeq 2.05m$ in the limit $N\to\infty$. This value approximately agrees with the previous result by Oohara *et al.* who conclude that $L_{\rm crit}=2.0m$ [3].

In Fig. 4, we show the error for the estimation of $\eta$ of the common apparent horizon as a function of $N^{-1}$ for $L=1.5m$ and $2.0m$. This figure is obtained as follows: First, we determine the asymptotic value of $\eta$ at $N\to\infty$ (hereafter $\eta_{N\to\infty}$) assuming that $\eta$ behaves as $\eta_{N\to\infty}+C'N^{-2}$ for large $N$ where $C'$ is a constant, resulting in $\eta_{N\to\infty}$ being $6.60\times10^{-3}$ for $L=2m$ and $1.41\times10^{-3}$ for $L=1.5m$. Then, we plot $\eta-\eta_{N\to\infty}$ as a function of $N^{-1}$. The figure shows that the results are second-order convergent with increasing the grid number. We note that Oohara *et al.* computed $\eta=6.62\times10^{-3}$ for $L=2m$ [3], which is in good agreement with our result $\simeq 6.60\times10^{-3}$. The error of the area is approximately evaluated by $2\delta\eta$ where $\delta\eta$ denotes the error of $\eta$. Thus, even for $N=15$, the error for the estimation of the area is less than 0.1% for $L=1.5m$. For $L=2.0m$, the error for the estimation of the area is larger than that for $L=1.5m$, indicating that a large $N$ is necessary for highly nonspherical apparent horizons. However, the error is still at most $\sim 0.2\%$ for $N=30$. Therefore, for determining the area of the apparent horizon within $\sim 1\%$ error, $N=30$ appears to be a sufficiently large grid number.

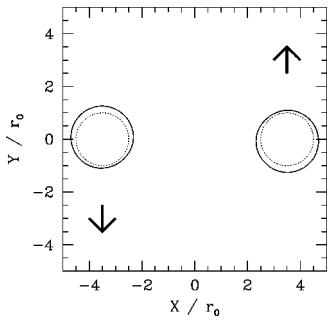


FIG. 5. Locations of apparent horizons (solid lines) for two orbiting black holes. The dotted lines denote surface of the dust balls. The arrow denotes the direction of the motion of the dust balls.

Finally, we apply this finder to an initial data of two orbiting black holes of equal mass to demonstrate that it works well even for time-asymmetric 3D space and numerical data sets. Data sets for binary black holes are obtained inputting a dense spherical dust matter and adding a uniform velocity field to the spatial component of the four velocity as $u_i = (0, Vx/|x|, 0)$ where $V$ is a positive constant. Here, we assume that the centers of mass of two dust balls are located along the $x$ axis. The parabolic density profile for $\rho_* \equiv \rho\psi^6\sqrt{1+V^2/\psi^4}$ where $\rho$ is the rest mass density is given for the dust balls as in [1] so that the momentum constraint can be solved analytically. On the other hand, the Hamiltonian constraint (i.e., the equation for $\psi$) is solved numerically as in [1]. We choose $(\varphi, \theta)$, identifying their center with the center of the dust balls, and give $h = 1.5r_0$ as the initial guess. As an example, in Fig. 5, we show the location of apparent horizons on the orbital plane (solid lines) for the case that the centers of the dust balls are located at $x = \pm 3.5r_0 \equiv x_c$, and the total rest mass, the Arnowitt-Deser-Misner (ADM) mass, and the total angular momentum of the system are $10r_0$, $6.8r_0$, and $35r_0^2$. Here, the dashed lines denote the surface of the dust balls, and all quantities are normalized by the radius of the dust balls $r_0$. We note that the apparent horizon is typically determined within 30 iteration steps for a wide range of $V \leqslant 0.5$ and $|x_c|/r_0 \leqslant 4$. It is interesting to report that the apparent horizons are shifted in the opposite direction to the moving direction due to the boost motion as shown in [13].

## IV. SUMMARY

We have briefly described a numerical method for finding apparent horizons in general 3D spaces of no symmetries. Showing numerical results for test problems, we have demonstrated that this code can determine the apparent horizon in general 3D spaces. It will be widely used in 3D numerical relativity, for example, to find the apparent horizon of a black hole formed after merger of binary neutron stars of unequal mass.

## ACKNOWLEDGMENTS

We started this work when M.S. visited SISSA. He thanks J.C. Miller, L. Rezzolla, and D.W. Sciama for their hospitality. Numerical computations were performed on the FACOM VX/4R machines in the data processing center of NAOJ. This work was supported by JSPS.

[1] M. Shibata, Phys. Rev. D **55**, 2002 (1997).
[2] T. Nakamura, Y. Kojima, and K. Oohara, Phys. Lett. **106A**, 235 (1984).
[3] K. Oohara, T. Nakamura, and Y. Kojima, Phys. Lett. **107A**, 452 (1985).
[4] M. Alcubierre, S. Brandt, B. Brügmann, C. Gundlach, J. Masso, E. Seidel, and P. Walker, gr-qc/9809004.
[5] T. W. Baumgarte, G. B. Cook, M. A. Scheel, S. L. Shapiro, and S. A. Teukolsky, Phys. Rev. D **54**, 4849 (1996).
[6] J. Thornburg, Phys. Rev. D **54**, 4899 (1996).
[7] M. F. Huq, M. W. Choptuik, and R. A. Matzner, gr-qc/0002076.
[8] M. Shibata, Prog. Theor. Phys. **101**, 1199 (1999); Phys. Rev. D **60**, 104052 (1999); M. Shibata and K. Uryū, *ibid.* **61**, 064001 (2000).
[9] M. Shibata, Prog. Theor. Phys. **101**, 251 (1999); M. Shibata, T. W. Baumgarte, and S. L. Shapiro, Phys. Rev. D **61**, 044012 (2000).
[10] Note that the surface of the apparent horizon is not always expressed by this form in general cases. Here, we restrict our attention to apparent horizons expressed by this form.
[11] Throughout this paper, we use units $c = 1 = G$ where $c$ and $G$ are speed of light and gravitational constant.
[12] D. R. Brill and R. W. Lindquist, Phys. Rev. **131**, 471 (1963).
[13] G. B. Cook and J. W. York, Jr., Phys. Rev. D **41**, 1077 (1990).